A simplified computational approach to hydrodynamic behavior of an ammonia-phosphoric acid mixing system within a tubular reactor

2 3 4

1

Halina Murasiewicz, Barbara Zakrzewska*

5

- 6 West Pomeranian University of Technology in Szczecin, Faculty of Chemical Technology
- 7 and Engineering, Department of Chemical and Process Engineering, Piastów 42, 71-065
- 8 Szczecin, Poland

9

10 *Corresponding author, e-mail: zakrzewska@zut.edu.pl

11

- 12 ORCID
- Halina Murasiewicz https://orcid.org/0000-0003-3603-7377
- 14 Barbara Zakrzewska https://orcid.org/0000-0001-7745-9272

1516

Abstract

- 17 This study employs a simplified computational approach to investigate the hydrodynamic
- behavior within tubular reactors for Monoammonium Phosphate (MAP) fertilizer production.
- 19 The main objective is to understand the impact of key parameters, including volumetric flow
- rates, fluid properties, reactor geometry, operating conditions, and distinct inlet configurations,
- 21 on reactant distribution and mixing efficiency. Two primary cases were investigated: Case 1,
- 22 where ammonia was injected coaxially with phosphoric acid introduced via a side inlet; and
- 23 Case 2, where phosphoric acid was injected coaxially with ammonia entering through a side
- 24 inlet. A significant effect of the reactant dosing location into the reactor was observed and was
- 25 more effective in Case 2 with respect to the MAP formation reaction. High ammonia and acid
- velocities were obtained at the constriction (nozzle) in the reactor tube. The nozzle design
- 27 caused a uniform discharge of the reactants to the further part of the reactor, where there was
- 28 good mixing of the components, comparable to Cases 1 and 2.
- 29 These simulations provide a practical tool for engineers to adjust design parameters, optimize
- 30 residence times, and ensure consistent product quality, facilitating both laboratory and

This article has been accepted for publication and undergone full peer review but has not been through the copyediting, typesetting, pagination and proofreading process which may lead to differences between this version and the version of record. Please cite this article as DOI: 10.24425/cpe.2025.155545.

Received: 07 July 2025 | Revised: 21 August 2025 | Accepted: 10 September 2025



industrial-scale applications. Future studies should incorporate chemical species transport and reaction kinetics to further enhance model accuracy and provide a more comprehensive understanding of the reaction process. Ultimately, this research offers valuable insights for informed decision-making in optimizing tubular reactor design and operation, leading to improved MAP production efficiency and product quality.

Keywords: tubular reactor, fertilizer MAP, CFD modelling, hydrodynamics

37

39

40

41

42

43

44

45

46

47

48

49

50

51

52

53

54

56

57

58

59

60

31

32

33

34

35

36

38 1. INTRODUCTION

The global demand for food security necessitates efficient and sustainable agricultural practices, with fertilizers playing a pivotal role in maximizing crop yields. Among these, Monoammonium Phosphate (MAP), a highly concentrated source of both nitrogen and phosphorus (Havelange et al., 2023), is a cornerstone of modern fertilization strategies due to its excellent solubility and nutrient availability. The production of MAP typically involves the exothermic reaction between ammonia and phosphoric acid, often carried out in specialized reactors designed to manage heat, ensure thorough mixing, and optimize reaction kinetics. There are a few methods for the production of MAP fertilizer and the most popular are: Tennessee Valley Authority (TVA) basic process (pre-neutralizer process); AZF (Now Grade Paroisse) process (dual- pipe reactor process) with the N:P ratio equalled at 1.05; ERT-Espindesa Technology with an adjusted molar ratio of NH₃: H₃PO₄ to obtain required product; Jacobs slurry process (a combination of pre-neutralizer and pipe reactor) and others (UN Industrial Development Organization, 1998). Details information about aforementioned processes are presented in (Nyers et al., 1979, UN Industrial Development Organization, 1998). Generally, MAP is prepared by the exothermic reaction of liquid phosphoric acid (H₃PO₄) and anhydrous ammonia (NH₃) in the one-to-one ratio, as represents below

55
$$H_3PO_4 + NH_3 \rightarrow NH_4H_2PO_4 (MAP) + Q$$
 (1)

but when the mole ratio between nitrogen and phosphorus is 2, then diammonium phosphate (DAP) is formed. The slurry product of the reaction is either solidified in a granulator (dual pipe reactor process: one located in a granulator and second in a dryer) or heat of the reaction caused evaporation of water and then solidified MAP (single pipe reactor located in the granulator). At the same time as the main reaction (1), the side reactions occur in the pipe

- reactor due to some amount of contaminates such sulphates, iron and silicon compounds existed in H₃PO₄:
- $H_2SO_4 + 2NH_3 \rightarrow (NH_4)_2SO_4$ (2)

$$H_2SiF + 2NH_3 \rightarrow (NH_4)_2SiF \tag{3}$$

- The production process of MAP/DAP in unaffected by the side reactions. Solid MAP is rather in needle shape of the tetragonal form (Gargouri et al., 2012) with chemical properties presented in (Chemical Book, 2025) and equivalent content of P_2O_5 in MAP typically varies between 48–61% depending on the scale of impurities in H_3PO_4 . In many cases, granules of MAP fertilizer are coating by polymers to enable and improve the utilization of the nutrients of plants and crops (Kabiri et al., 2020) and to diminish fertilizer losses and minimize environmental pollution. The main benefit of manufacturing of MAP compared with other phosphorus fertilizers is the possibility of using a low-quality phosphorous acid. The interest of this fertilizer is due to the fact that MAP that is easily water-soluble and dissolves rapidly in sufficiently moist soil. Upon dissolution separates and releases ammonium (NH₄⁺) and phosphate ($H_2PO_4^-$) which both are import for healthy and sustained plants growth.
- Over the past two decades, there has been a large number of studies of MAP particularly focusing on influence on different plantations (Andrade et al., 2020; Eltarabily et al., 2019); strategy of production of phosphate fertilizer with different rate of release of nutrients (Kabiri et al., 2020; Timilsena et al., 2015); the physicochemical characterization of MAP fertilizer (Gargouri et al., 2010); coating materials used for MAP granules (Bortoletto-Santos et al., 2018; Kabiri et al., 2020; Lino et al., 2018); the structure and characterization of crystals/struvite, growth and crystallisation process (Gargouri et al., 2012; Liu et al., 2011; Lombi et al., 2004; Mpountas et al., 2017; Xue et al., 2013), mainly on the improvement of agronomic effectiveness and impact on an environment of MAP fertilizer. However, there is, surprisingly, less insight at the entire production process, especially at the 'key apparatus' in MAP plant - a cross-pipe reactor, where the reaction takes place and depending on its yield the product is obtained. There is no details information about the hydrodynamic of the two-phase flow of aqueous and vapour phase and transport mechanism occur in a reactor, which is important for a product formulation. It is very difficult and probably impossible because of cost experimentally investigate hydrodynamic in a pipe reactor in any plant but computational fluid dynamics (CFD) can help in solving this problem since allows to simulate a turbulent flow together with the reaction in

real size of apparatus and provide better understanding of the flow patterns, mixing behaviour and impact velocity of phosphoric acid on product (MAP). Recently, significant improvement in computational power allows treating CFD as a viable non-invasive tool for understanding the complex phenomena which occur in gas and liquid phases in any 3D geometry. The application of CFD has met with great success in many problems even sophisticated due to the recent development of high-performance computers as was proven by numbers of publications over the past decade.

Many records (mostly patents) found in the literature assessed to the tubular reactor are focused on the process parameters (Hebei Toprun Chemical Industry, 2004; Shanghai Research Institute of Chemical Industry SRICI, 2006; Tennessee Valley Authority, 1987), modification of the construction of reactor (Belis et al., 1986; Yara International ASA, 2005) but do not particularly on flow pattern and mixing in a tubular reactor. The question naturally arises is how hydrodynamics and mixing process occur in a tubular reactor can influence and improve the manufacture of monoammonium phosphate fertilizers which are considered relatively important because this material is widely produced granular phosphate fertilizer in the world today.

The study presented herein deals with the numerical simulation of turbulent flow in the tubular reactor using in MAP production. The aim of this work is a theoretical examination of the turbulent flow of the two-phase system consisted of gas and liquid phases, mixing process in the tubular reactor under the process conditions similar to those applied in the fertilizer manufacturing. Understanding into transport characteristics within a gas-liquid flow is of vital importance for the design, operation and optimization of such tubular reactor. However, to the best of our knowledge, there is no comprehensive analysis so far of the flow of the turbulent gas-liquid system in tubular reactor used for MAP fertilizer production. The investigation of a hydrodynamic in the tubular reactor from a modelling perspective is appealing and promising to derive a fully predictive model. Simplified computational methods offer a practical and cost-effective approach to understanding the hydrodynamic behavior within a tubular reactor used in MAP fertilizer production. By focusing on key parameters and utilizing existing correlations, these methods can provide valuable insights for optimizing reactor design, process control, and troubleshooting.

In this work, computational fluid dynamics (CFD) was used to analyze single-phase velocity profiles of both ammonia (as gas) and phosphoric acid (as liquid) independently in the reactor

geometry. This simplified approach allows for a focused investigation into the fundamental hydrodynamic phenomena, such as fluid acceleration through nozzles, mixing characteristics of different inlet designs, and the development of velocity profiles over time. By dissecting the individual flow behaviors, we aim to lay the groundwork for understanding the more complex multiphase reactive flow, providing critical insights into reactor design optimization for enhanced MAP production efficiency and safety.

130 2. THEORETICAL

124

125

126

127

128

129

131

132

133

134

135

136

137

138

139

140

141

142

143

144

145

146

147

148

149

150

151

152

153

154

155

Turbulent multiphase flows (liquid-liquid, gas-liquid and others) are much common than single flow and it can be found in a number of important industrial applications, particularly in the oil, process, cosmetic, fertilize, and chemical industries. There are many examples of operations with this type of systems such heterogeneous, solvent extractions, emulsion and suspension polymerization, emulsification and fermentation. The knowledge about drop size and drop size distribution (DSD) and nature of their modification may have a significant impact on the process intensification and control and on the quality of the product. The size of droplets either solid particle or bubble may change due to the transport processes and chemical reaction which might occur in a system. The entire process of changes of droplets/particles might be combination of different phenomena which are nucleation, growth, coalescence, decomposition, aggregation and disintegration of the dispersed phase and others. A full description of a two-phase system together with conservation/balance equations of momentum, mass or energy causes increasing of the number of equations and requires high computation performance. For example, when turbulent multiphase system consists of liquid and gas phases coupled with turbulence is examined, many complex and interacting physical phenomena as surface tension, dispersed phase-turbulence interaction, coalescence and breakage, separation effects, and wall interactions might characterize it. This causes both description and computation of these models very difficult. CFD approach gives a simplified and wellestablished alternative for describing dispersed flows by so-called Eulerian-Eulerian multifluid model, mixture model and volume of fluid (VOF). Mixture model solves one continuity and momentum balance equation for the mixture of the different phases existed in the system (based on mixture properties). The phases can move with different velocities by using the concept of slip velocity. For example, in a liquid-gas system, the velocities for both phases are calculated by taking the assumption that the gas-liquid system reaches equilibrium conditions locally and instantaneously underneath the impact of the different forces that influence upon it.

- Example of applications to multiphase systems of algebraic mixture model (algebraic equations
- to determine the phase velocities) called the algebraic slip model (ASM) seems to be promising
- 158 (Icardi et al., 2014; Rzehak et al., 2012).
- Volume of fluid (VOF) method belongs to Eulerian method and it has been extensively applied
- in predicting various two-phase fluid flows (Edelbauer, 2017). In this method two or more fluids
- do not interpenetrate each other. Application of this method allows to follow the shape and
- position of the surface.
- 163 The Eulerian–Eulerian multi-fluid model is the most complex model used to a multiphase
- system in Ansys Fluent. This widely used approach is, in fact, probably due to its compromise
- between computational cost, a number of details provided and easily applicability. The multi-
- 166 fluid approach is appropriate for separated flows where both phases can be described as a
- 167 continuum and it can also be applied to simulate dispersed flows when the total motion of
- particles is desirable rather than a single particle (Jakobsen, 2008). In the Eulerian–Eulerian
- multi-fluid model a set of conservation equations is numerically solved for each phase and
- phases are treated as interpenetrating continua. Coupling between the phases is accomplished
- by the pressure and interphase exchange coefficients, which need to be modelled. The way of
- coupling is handled depends upon the type of phases involved, i.e. differently for fluid-solid
- 173 (granular) flow than fluid-fluid (non-granular) flow. However, the number of equations that
- need to be solved especially for the very complex systems might be the one of limitation of
- using this method because of high computational costs and convergence issues (Prosperetti and
- Jones, 1987). This method can be applied for simulation of bubble columns, particle
- suspensions or fluidized beds and suitable for dense flows (high value of volume fraction of
- dispersed flow). All the advantages of this method make it particularly valuable in two phase
- simulation therefore it was implemented in the current numerical study.
- The governing mass (Eq. 4) and momentum (Eq. 5) equations for a two-phase model are shown
- 181 below:

$$182 \quad \frac{\partial}{\partial t}(\rho_k \alpha_k) + \nabla \cdot (\rho_k \alpha_k \overline{u}_k) = 0 \tag{4}$$

183
$$\frac{\partial(\rho_k \alpha_k \overline{u}_k)}{\partial t} + \nabla \cdot (\rho_k \alpha_k \overline{u}_k \overline{u}_k) = -\alpha_k \nabla P + \nabla \cdot \left(\alpha_k \mu_{eff,k} (\nabla \overline{u}_k + (\nabla \overline{u}_k)^T)\right) + \rho_k \alpha_k g + F_k \quad (5)$$

- where ρ_k , α_k , \overline{u}_k are density, volume fraction and mean velocity of kth phase, respectively, P is
- the mean pressure shared by the two phases, \overline{u}_k is the mean velocity field. Both phases: liquid
- and gas are assumed to occupy space proportional to their volume so that their volume fractions
- sum equal one in the cells domain (Kerdouss et al., 2006). The term F_k in Eq. 3 represents the
- interphase momentum exchange terms between liquid (l) and gas (g) phase and its responsible

- for the interaction between phases (Dhanasekharan et al., 2005). Here, the term F_k is reduced
- to the drag force proportional to the mean velocity difference of both phases given by (Eq. 6):

$$F_l = -F_g = K(\overline{u}_g - \overline{u}_l) \tag{6}$$

- 192 K is defined as the interphase momentum exchange coefficient and it can be written as
- 193 follows:

194
$$K = \frac{3}{4}\rho_l \alpha_l \alpha_g \frac{c_D}{d_h} |\overline{u}_g - \overline{u}_l|$$
 (7)

- The variable d_b means the droplet diameter of dispersed phase and C_D is the drag coefficient
- defined by standard correlation of Schiller and Naumann (Schiller and Naumann, 1935) as

197
$$C_D = \begin{cases} \frac{24(1+0.15Re_z^{0.687})}{Re_z} & Re_z \le 1000\\ 0.44 & Re_z > 1000 \end{cases}$$
 (8)

The Re_z represents the relative Reynolds number written as

$$Re_z = \frac{\rho_l d_b |\overline{u}_g - \overline{u}_l|}{\mu_l} \tag{9}$$

- 201 The Reynolds-Averaged Navier-Stokes equations (RANS) method was used in current
- investigation with the dispersed k- ε turbulence model (Launder and Spalding, 1972) given by
- 203 the following equations:

$$204 \quad \frac{\partial}{\partial t}(\rho_m k) + \nabla \cdot (\rho_m \overline{u}_m k) = \nabla \cdot \left(\frac{\mu_{eff,m}}{\sigma_k} \nabla k\right) + P_{k,m} - \rho_m \varepsilon \tag{10}$$

$$205 \quad \frac{\partial}{\partial t}(\rho_m \varepsilon) + \nabla \cdot (\rho_m \overline{u}_m \varepsilon) = \nabla \cdot \left(\frac{\mu_{eff,m}}{\sigma_{\varepsilon}} \nabla \varepsilon\right) + \frac{\varepsilon}{k} \left(C_1 P_{k,m} - C_2 \rho_m \varepsilon\right)$$
(11)

- where velocity, density, effective viscosity and turbulent kinetic energy were assumed as for
- 207 mixture and $P_{k,m}$ is the rate of production of turbulence kinetic energy.
- The turbulent viscosity, $\mu_{t,m}$, is computed from

$$\mu_{t,m} = \rho_m C_\mu \frac{k^2}{s} \tag{12}$$

- The value of parameters in these equations are assigned the same as those for the standard k- ε
- 211 model: $C_{\mu} = 0.09$; $C_1 = 1.44$; $C_2 = 1.92$; $\sigma_k = 1$; $\sigma_{\varepsilon} = 1.314$ (Launder and Spalding, 1972).
- The turbulence model solves a set of k and ϵ transport equations for each phase (along with
- standard wall function), which is important when the turbulence transfer between the phases
- 214 plays a dominant role. The problem was numerically solved with a commercial CFD code
- 215 Ansys FLUENT 19 which relays on the finite volume method used to convert the governing
- 216 equations to algebraic equations that can be solved mathematically.

This section is dedicated to describing the geometry and the type of mesh used in the current study. The boundary conditions and the numerical procedure are also presented.

3.1. Geometry and Mesh

The solution domain, similar to this used in fertilizer plant, investigated in this study is presented in Figure 1. Firstly, the 3D Cartesian framework geometry and then mesh was created in Gambit 2.4.6 - the FLUENT pre-processor. Two numerical mesh with a fine mesh 3.3M and a coarse mesh 500k tetrahedral cells were generated. It is essential for numerical calculations to gain a grid-independent solution so that a grid sensitivity study must be performed. The quality of a mesh might be evaluated by quality criterion such aspect ratio, skewness or refine the mesh until the difference between two solutions reaches zero (Picardi et al., 2016). The quality of meshes was examined using the skewness criteria based on the difference between the cell size and the optimal size which is the equilateral volume. All the cells skewness is below 0.70 which indicate that the mesh is acceptable.

Furthermore, a mesh independence study was conducted to ensure that the numerical solution was not dependent on the grid resolution. Preliminary simulations were executed on both grids

Furthermore, a mesh independence study was conducted to ensure that the numerical solution was not dependent on the grid resolution. Preliminary simulations were executed on both grids to evaluate key parameters. The results of these studies are presented in the Results section in subchapter 4.1. Based on these preliminary simulations, it was decided to use a 500k cells grid for further numerical studies.

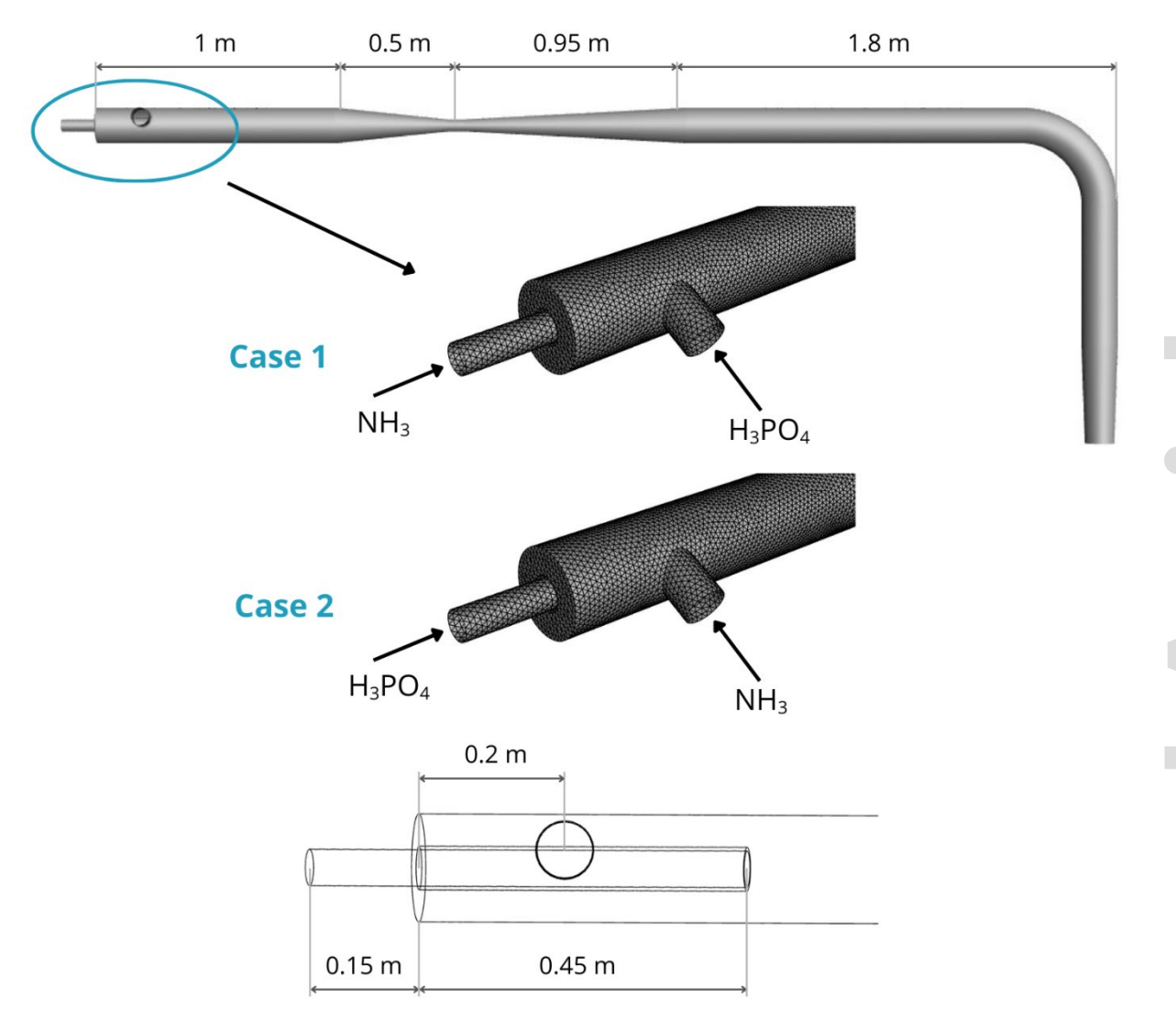


Figure 1. Solution domain of pipe cross reactor and unstructured mesh used in the model (500 k cells).

The dimensions of the reactor are similar to this used in MAP production which is composed of two inlets, separately for ammonia (gas) and phosphoric acid (liquid, 69% in H₂O) and one outlet for the product of the reaction. The reactor diameter was 0.15 m. The diameter of the front inlet was 0.073 m and for the side inlet was 0.05 m. The reactor length in the horizontal part is 4.4 m (including inlet), while the length of the discharge pipe is 1.4 m. The reactor outlet pipe tapers slightly and the outlet diameter was 0.12 m. The main reactor tube has a 0.05 m diameter nozzle at a distance of 1.5 m from the inlet.

3.2. Boundary conditions

In this work, the effect of ammonia and acid inlet location was studied in two cases (Figure 1):

- Case 1: ammonia was supplied to the reactor from the front of the reactor whereas orthophosphoric acid flows through side inlet as is presented in (Hudson and Pendergrast, 1975).
 - Case 2: phosphoric acid flowed through the main inlet and ammonia through the side inlet. The boundary conditions and properties of orthophosphoric acid and gaseous ammonia at the reactor inlets are summarized in Table 1.

Table 1. Properties of orthophosphoric acid and gaseous ammonia at the reactor inlets.

Variables	Case 1		Case 2	
	H ₃ PO ₄ (69% in H ₂ O)	NH ₃ (gas)	H ₃ PO ₄ (69% in H ₂ O)	NH ₃ (gas)
Inlet diameter [m]	0.073	0.05	0.05	0.073
Density [kg/m³]	1521	4.859	1521	4.859
Viscosity [Pa·s]	0.04	1.015·10 ⁻⁵	0.04	1.015·10 ⁻⁵
Pressure [bar]	6	6	6	6
Temperature [°C]	20	20	20	20
Mass flowrate [kg/s]	13.205	1.711	13.205	1.711
Molar flowrate [kmol/s]	0.286	0.101	0.286	0.101
Inlet velocity [m/s]	2.074	177.833	4.422	83.427
Reynolds number	5.76·10 ⁴	4.29·10 ⁶	8.40·10 ⁴	$2.94 \cdot 10^6$

In both cases the continuous phase was gaseous ammonia and the dispersed phase was orthophosphoric acid (69% in H₂O). The inflow conditions were defined separately for two inlets (Table 1) where ammonia and phosphorous acid velocities were fixed from the daily MAP production capacity of 1000 t MAP/day (11.574 kg/s) to obtain a more realistic and accurate representation of what occurs in the process. Based on the MAP formation reaction (Eq. 1) and the assumed MAP production capacity (11.574 kg/s), the ammonia and orthophosphoric acid consumption and also inlet velocities, respectively, were calculated for the two studied cases (Table 1). The boundary conditions for the inlet of gaseous ammonia, which is defined as the continuous phase, were set as *inlet velocities*. For Case 1, the gas velocity was 177.8 m/s (with a null velocity for the liquid phase). For Case 2, the gas velocity was 83.43 m/s. This change in velocity is a direct result of the larger inlet diameter used in Case 2, as a larger area for a constant mass flow rate leads to a lower velocity. These inlet velocities

for ammonia seem high. However, in the real process, liquid ammonia is supplied to the reactor instead of gaseous ammonia. Then the velocities would be 1.37 m/s and 6.65 m/s, respectively. This is due to the large difference in the density between liquid and gaseous ammonia. Due to the exothermic reaction (Eq. 1) and high temperature in the reactor, liquid ammonia practically immediately evaporates after entering the reactor. If we wanted to include this phase transition in the model, it would be more complicated. Therefore, we decided to simplify the model and assumed that the ammonia at the inlet would be in the gaseous state, i.e. after evaporation. Hence such high velocities of ammonia at the reactor inlet. The primary objective was to validate the computational fluid dynamics (CFD) model's ability to accurately capture the key hydrodynamic behavior and mixing patterns of the two-phase flow at the point of initial contact. By employing an isothermal assumption, we were able to isolate the fluid dynamics from the thermal effects, allowing for a focused analysis and validation of the core flow field and mixing predictions. It is acknowledged that temperature variations resulting from the heat of reaction will influence fluid properties such as density and viscosity, thereby affecting the flow field. Therefore, incorporating the energy equation to account for these thermal effects and provide a more comprehensive simulation is a planned and crucial next step for future research. The volume fraction of dispersed phase corresponded to 0. The two-phase system is formulated here much different that usually finds in the literature, where in many cases gas (bubble) phase is dispersed in a liquid continuous phase. Typically, this system is found in bioreactors, packed or bubble columns. Here, we consider a case that is characterized by one continuous gas phase that coexists with a dispersed liquid phase. It means that liquid droplets are entrained by the gas-phase since the velocity of the gaseous phase is much larger. In fact, droplets are always characterized by their different sizes, which results in a drop size distributions (DSDs), which varies among points in the flow since many phenomena are involved, e.g., convection, turbulent dispersion, coalescence, breakage, and mass transfer. Thus, it would be interesting to determinate droplets size distributions (DSDs) in the crucial points of investigated reactor, e.g. by using population balance equations (PBEs) (Ramkrishna, 2000) or standard method of moments (SMM). However, this is beyond the scope of this paper. Therefore, here the simple approach for modelling a two-phase flow (as mentioned above) was adopted without determined the size of liquid at the inlet and its evaluation in the entire volume of the reactor. The boundary conditions for second inlet, where H₃PO₄ is supplying to the reactor, was fixed as velocity inlet with the value of velocity assumed to 2.07 m/s for Case 1 and 4.42 m/s for Case 2. and volume fraction of dispersed phase was 1 for two cases.

271

272

273

274

275

276

277

278

279

280

281

282

283

284

285

286

287

288

289

290

291

292

293

294

295

296

297

298

299

300

301

302

304 A boundary condition for reactor outlet was used at the *outflow* with a flow rate weighting 305 corresponded 1. The boundary conditions for the wall was set as a stationary wall with the 306 roughness factor equalled 0.5. A no-slip condition is fixed, and it means that the velocity is set 307 to 0 m/s.

3.3. *Model*

308

314

315

316

317

318

319

320

321

322

323

324

325

326

327

328

329

330

331

332

333

334

335

336

- 309 The numerical model has been designed using the following hypotheses:
- 310 The flow is Newtonian, viscous and incompressible for both phases since Icardi et al. 311 (2014) have proven that a compressible solver gives very similar results for a gas phase.
- 312 The flow is considered isothermal and turbulent based on the value of Reynolds number 313 calculated for two-phase system.
 - The effect of the surface tension is neglected.

A simplified approach for a two-phase flow simulation assumes a fixed droplet diameter of 0.001 m. While this hypothesis is used by many researchers, it does not fully reflect reality. The VOF method requires that the size of a single droplet be larger than the numerical cell size to ensure accurate representation. In the current study, the computational grid's cell size ranged from a minimum of 0.003 m to a maximum of 0.008 m. Given the assumed droplet diameter, the dispersed phase was not adequately resolved by the grid. It is acknowledged that this limitation may impact the accuracy of results and affect the calculation of phenomena such as droplet breakup and coalescence. However, this assumption was maintained as a preliminary step to investigate the overall hydrodynamic behavior, while a more refined approach is beyond the scope of this investigation. The above equations were solved by using commercial CFD package Ansys Fluent 19 together

with appropriate boundary condition, as aforementioned. The flow model is based on solving Navier-Stokes equations for the Eulerian-Eulerian multiphase model along with dispersed multiphase turbulent model. All governing equations were iteratively computed to the discrete form of the mathematical model. Phase Couple SIMPLE algorithm, which is an extension of SIMPLE algorithm for multiphase flow (Patankar, 1980) was applied for pressure-velocity coupling together with first order implicit formulation for unsteady formulation. First-order upwind scheme was used for discretization of spatial derivatives. The numerical simulations were performed for a time period of 3 s. This duration is significantly longer than the calculated residence time of approximately 0.215 seconds for both cases. This intentional difference is crucial for the simulation's accuracy. The 3-second simulation time was selected to ensure that the fluid flow reached a steady-state condition. This is a standard practice CFD to guarantee

that the final solution is stable and not influenced by initial transient effects. Therefore, this computational duration does not represent the physical residence time of the fluid. Instead, it confirms that the flow field is fully developed and the numerical solution is reliable. The time step of 0.001 s was set to avoid numerical difficulties. The number of iterations per time step equalled 300 which was adjusted based on preliminary study. It was assumed that the converged solution was reached when scaled residuals of all variables were smaller than $1 \cdot 10^{-6}$.

Due to the complexity of the system and the number of coupled models, a solution was firstly gained using Euler-Euler approach with the fixed droplet size. This approach allowed to avoid instabilities and improve convergence.

346 4. RESULTS

4.1 Grid independence test

A grid independence study is a crucial step in computational fluid dynamics (CFD) and other numerical simulations. Its purpose is to ensure that the solution obtained is not a function of the mesh resolution. The core principle is to demonstrate that further refinement of the mesh will not yield a significantly different result, thus confirming that the solution is accurate and reliable. This process is essential for balancing computational cost with the required level of solution accuracy. Results of the grid independence study are presented in Figure 2.

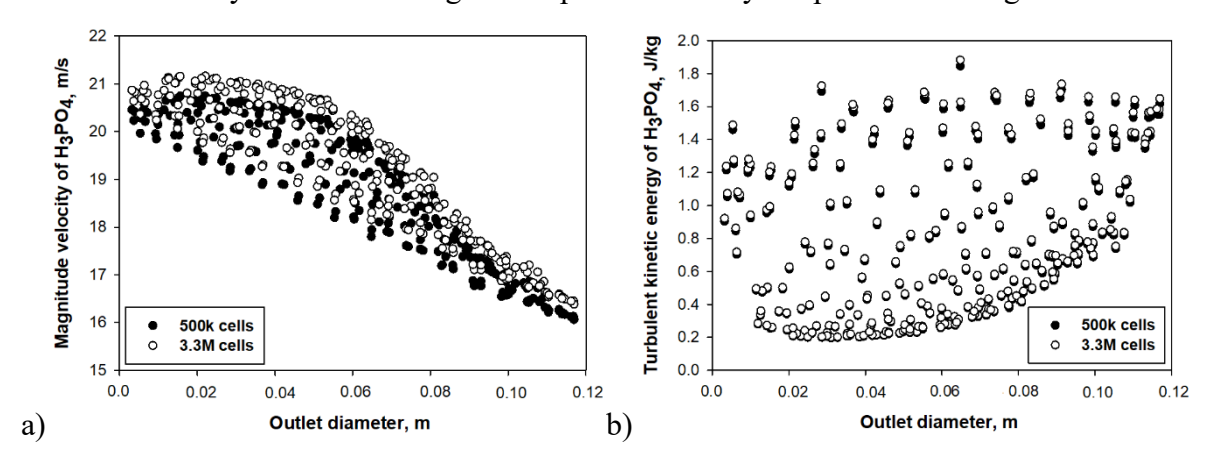


Figure 2. Mesh independence study comparing the 500,000-cell mesh and the 3.3-million-cell mesh. (a) magnitude velocity of H₃PO₄, (b) turbulent kinetic energy of H₃PO₄ as a function of distance along the reactor outlet.

A comparative analysis of the velocity fields for both meshes revealed that the core flow patterns and recirculation zones were in good qualitative and quantitative agreement. The spatial distributions (along the reactor outlet) and maximum magnitudes of the velocity fields showed minimal differences, indicating that the coarse mesh was sufficiently refined to

accurately resolve the bulk fluid dynamics. For instance, at a distance of 4.34 m, the estimated velocity magnitude is approximately 17.5 m/s for the 500k mesh and 17.4 m/s for the 3.3M mesh, representing a difference of less than 1%.

Similarly, a comparison of the turbulent kinetic energy (TKE) demonstrated a negligible difference in both values and distribution throughout the reactor. At a distance of 4.34 m, the

approximately 1.45 J/kg. This difference is approximately 3.5%, which is within acceptable limits for a mesh independence study. This confirmed that the 500,000-cell grid was capable of

estimated TKE for the 500k mesh is around 1.4 J/kg, while the value for the 3.3M mesh is

capturing the key turbulent characteristics of the system without the need for a higher cell count.

Based on these findings, it was concluded that the 500,000-cell mesh provided an optimal balance between computational accuracy, efficiency and simulation time. Consequently, this

373 grid was selected for all subsequent numerical studies, providing confidence that the results

were independent of the grid resolution. Additionally, the use of a coarse mesh (500k cells)

375 significantly reduced computational time.

4.2. Flow pattern in gas-liquid flow in pipe cross reactor

The hydrodynamic behavior of gas-liquid flow within a pipe cross reactor is a complex phenomenon, and understanding the governing parameters is crucial for effective reactor design and operation. These factors directly impact real-world performance metrics like mixing efficiency, phase separation, and ultimately, the yield and selectivity of chemical reactions.

Firstly, volumetric flow rates of the gas and liquid phases are of paramount practical importance. Adjusting these flow rates is often the primary lever operators use to control flow regimes. For example, in a reactor designed for a specific reaction, maintaining the correct gasto-liquid ratio (achieved by controlling flow rates) is essential to prevent flooding, ensure adequate contact between reactants, and optimize mass transfer. If flow rates are too low, reactants may not mix effectively; if they're too high, the reactor may become unstable or inefficient.

Secondly, the physicochemical properties of the fluids dictate how the phases interact, and this has significant practical implications. For instance, in processes where temperature varies, changes in viscosity can dramatically alter flow patterns, potentially leading to channeling or poor mixing. Similarly, interfacial surface tension is critical in processes involving droplet formation or foam generation, which can affect separation efficiency in downstream units. In practice, these properties often need careful consideration during process design and control.

Thirdly, reactor geometry and configuration are fundamental to achieving desired hydrodynamic behavior. The dimensions of the pipe, the angle of the cross, and the internal

design (e.g., baffles, packing) are all design choices that directly influence flow patterns, mixing, and residence time. In a practical setting, these design parameters are optimized to maximize the efficiency of the reactor for its intended purpose. Finally, the initial phase distribution and injection methods are crucial for establishing the desired flow regime from the outset. How the gas and liquid are introduced into the reactor (e.g., through nozzles, distributors) significantly impacts mixing, phase dispersion, and the uniformity of the flow. In practical applications, careful design of injection systems is necessary to ensure efficient and consistent reactor performance. For example, in a reactor designed for emulsion polymerization, the injection method can significantly affect the particle size distribution of the product. In the case of a tubular reactor, two-phase flow modeling of the gas-liquid type was carried out. In this case, all defined model equations were solved simultaneously from the beginning of the simulation. The calculations were very time-consuming and were carried out until a simulation time of 3 s was achieved. Furthermore, a simulation of only turbulent two-phase flow was performed simultaneously, which significantly reduced the computation time. Two-phase (gas-liquid) flow simulations were conducted within a tubular reactor to investigate the hydrodynamic behavior of the system. In the current study, the simulation was performed without chemical reaction to thoroughly assess the flow behavior within the tubular reactor. The analysis centered on evaluating the changes in velocity and the volumetric fraction distribution of the media within the two configurations: Case 1 and Case 2 (see Figure 1). This was conducted to simulate the replacement of the ammonia inlet and, subsequently, the associated ammonia inlet velocity. Figure 3 and Figure 4 present the temporal evolution of the average H₃PO₄ and NH₃ velocity distribution within the reactor, visualized as instantaneous velocity maps at successive simulation time t = 1.0 s for both cases. As variations in the simulation outcomes for differing durations were deemed marginal, the data presented herein specifically reflects the state at 1.0 second. Nevertheless, velocity profiles were comprehensively sampled and evaluated throughout the simulation interval of 0.6 to 3.0 s. The velocity contours delineate regions of maximum and minimum values, enabling the

characterization of flow dynamics and highlighting the influence of inlet conditions.

396

397

398

399

400

401

402

403

404

405

406

407

408

409

410

411

412

413

414

415

416

417

418

419

420

421

422

423

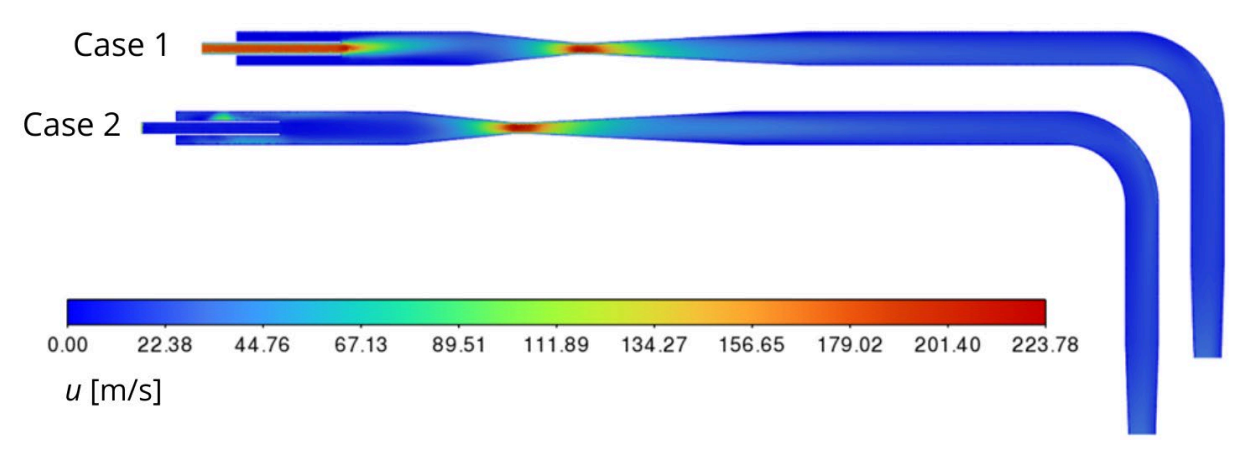


Figure 3. The distribution of average ammonia velocity of a tubular reactor for t = 1.0 s.

429

430

431

432

433

434

436

437

438

439

440

441

442

443

444

445

446

447

448

449

450

425 426

> As depicted in Figure 3, gaseous ammonia is injected coaxially with the reactor geometry at a velocity of approximately 177 m/s for Case 1. This high initial kinetic energy is visible as the prominent high value of velocity extends from the inlet into the initial converging section. As this already fast-moving stream enters the narrowest part (the nozzle) of the convergingdiverging nozzle, it undergoes further, albeit less dramatic, acceleration. The velocity in the nozzle reaching the highest values shown on the scale (approaching 223.78 m/s). This suggests that the nozzle is still providing significant acceleration, but the flow is already highly energetic upon entry.

435

In contrast, in Case 2 ammonia is injected through the side inlet at a velocity of approximately 83.43 m/s. As these moderately fast stream enter the nozzle, it experience a much more substantial acceleration compared to Case 1. The value of velocity rapidly transitions initial value to the maximum in the nozzle, indicating a significant increase in kinetic energy imparted by the nozzle. The peak velocities achieved in the nozzle visually appear to be comparable to those in Case 1 (approaching 223.78 m/s).

Case 1 starts with a high initial kinetic energy. The nozzle's role is to provide additional, though proportionally smaller, acceleration to reach the peak velocity. Case 2 begins with a moderate initial kinetic energy. The nozzle is responsible for a much larger proportion of the total acceleration, bringing the flow from a moderate speed to a very high peak velocity. This design is more typical if the upstream flow is at a lower velocity and significant acceleration is required within the reactor.

Despite the substantial difference in initial injection velocities of ammonia (177 m/s vs. 83.43 m/s), both Case 1 and Case 2 achieve remarkably similar peak velocities in the nozzle of the converging-diverging nozzle. The difference is in the velocity distribution from the inlets to the

nozzle for these cases. This clearly indicates that the design of the inlet section, as well as the nozzle itself, have a strong influence on the way the phases flow and spread in the area from the inlet to the nozzle and on the maximum velocity achieved in this part of the reactor. In the presented work, conditions without a chemical reaction are studied.

Beyond the high-velocity nozzle, the velocity distribution in the expanding section and around the 90-degree bend appears qualitatively similar for both cases. This reinforces the idea that the nozzle effectively homogenizes and dictates the downstream flow characteristics, minimizing the long-range impact of the differing inlet conditions.

As shown in Figure 4, H₃PO₄ is introduced into the reactor from the side opposite to the ammonia inlets. In both cases, the H₃PO₄ enters at low velocities compare to ammonia. As the flow progresses from the wider inlet section into the narrow nozzle of the converging-diverging nozzle, the velocity significantly increases. This acceleration is a direct consequence of the reduction in cross-sectional area. The peak velocities in the nozzle approaching the maximum velocity of 83 m/s, as seen in Figure 4 for both cases. The velocity profiles in the expanding section and through the bend are qualitatively similar for both cases, suggesting that the differences in the initial converging geometry do not significantly alter the flow behavior far downstream from the nozzle.

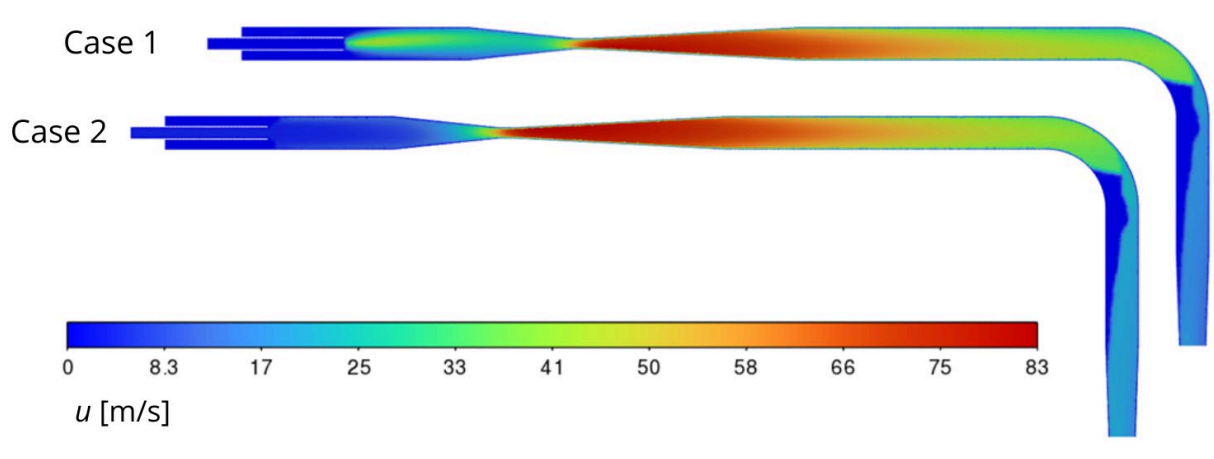


Figure 4. The distribution of average H_3PO_4 velocity of a tubular reactor for t = 1.0 s.

Similar to previous analyses, the velocity distribution around the 90-degree bend shows the flow conforming to the curve, with potentially slightly higher velocities along the outer radius of the bend. The comparison between Case 1 and Case 2 suggests that while the exact point of initial acceleration might differ slightly due to variations in the converging geometry, the ultimate peak velocity achieved in the nozzle and the downstream flow patterns remain

consistent. This indicates that the overall nozzle design is robust in achieving the desired high-velocity flow.

The interaction between the ammonia (NH₃) gas and orthophosphoric acid (H₃PO₄) liquid streams within the tubular reactor results in a pronounced acceleration and distribution of the acid. This is primarily driven by entrainment, where the higher velocity NH₃ gas drags the H₃PO₄ liquid, as clearly evident in the evolving velocity profiles shown in Figure 3 and 4. This flow behavior depends on several factors, including inlet conditions, where the angle and velocity of H₃PO₄ injection, as well as the shape and size of the inlet, significantly influence the initial distribution and subsequent interaction with the NH₃ gas flow. Two-phase flow dynamics also play a role, as entrainment, drag forces, and shear forces at the gas-liquid interface all contribute to the acceleration, breakup, and mixing of the H₃PO₄. Furthermore, fluid properties such as differences in density, viscosity, and surface tension between the NH₃ and H₃PO₄ phases affect momentum transfer, mixing, and the formation of droplets or films. Figure 5 presents a series of cross-sectional velocity profiles of ammonia at the reactor outlet for both Case 1 and Case 2, at four different time steps: t = 0.6; 1.0; 2.0 and 3.0 s. Results demonstrate the transient nature of the flow, particularly in the initial stages (Case 1, t = 0.6 s). The ammonia velocity stabilizes very quickly and from t = 1 s very similar velocity profiles were obtained.

495

477

478

479

480

481

482

483

484

485

486

487

488

489

490

491

492

493

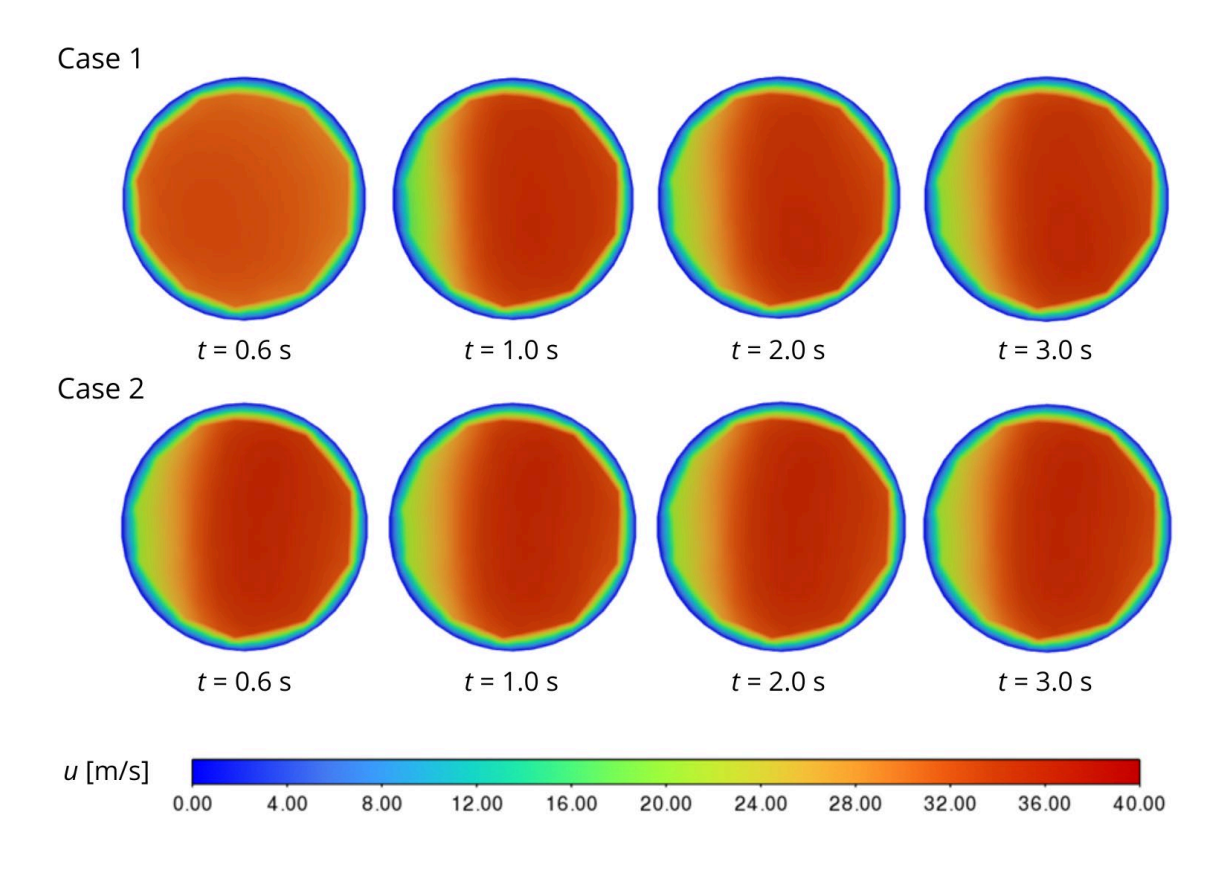


Figure 5. The distribution of average ammonia velocity at the outlet of a tubular reactor across different simulation time steps.

The similarity in the outlet profiles between Case 1 and Case 2, despite their differing inlet configurations (as seen in Figure 3), suggests that the reactor's internal geometry (specifically the nozzle and the bend) acts as an effective flow conditioner.

4.3 Dispersed phase volume fraction

An essential element of two-phase flow is the analysis of the dispersed phase's volume fraction, which allows for determining the mixing and distribution of the two reactants or the degree of segregation as they enter and interact within the initial section of the tubular reactor. Figure 6 illustrates the local volume fraction values of both phases: continuous - NH₃ and dispersed - H₃PO₄ for Case 1 and Case 2, at a simulation time of 2.0 seconds.

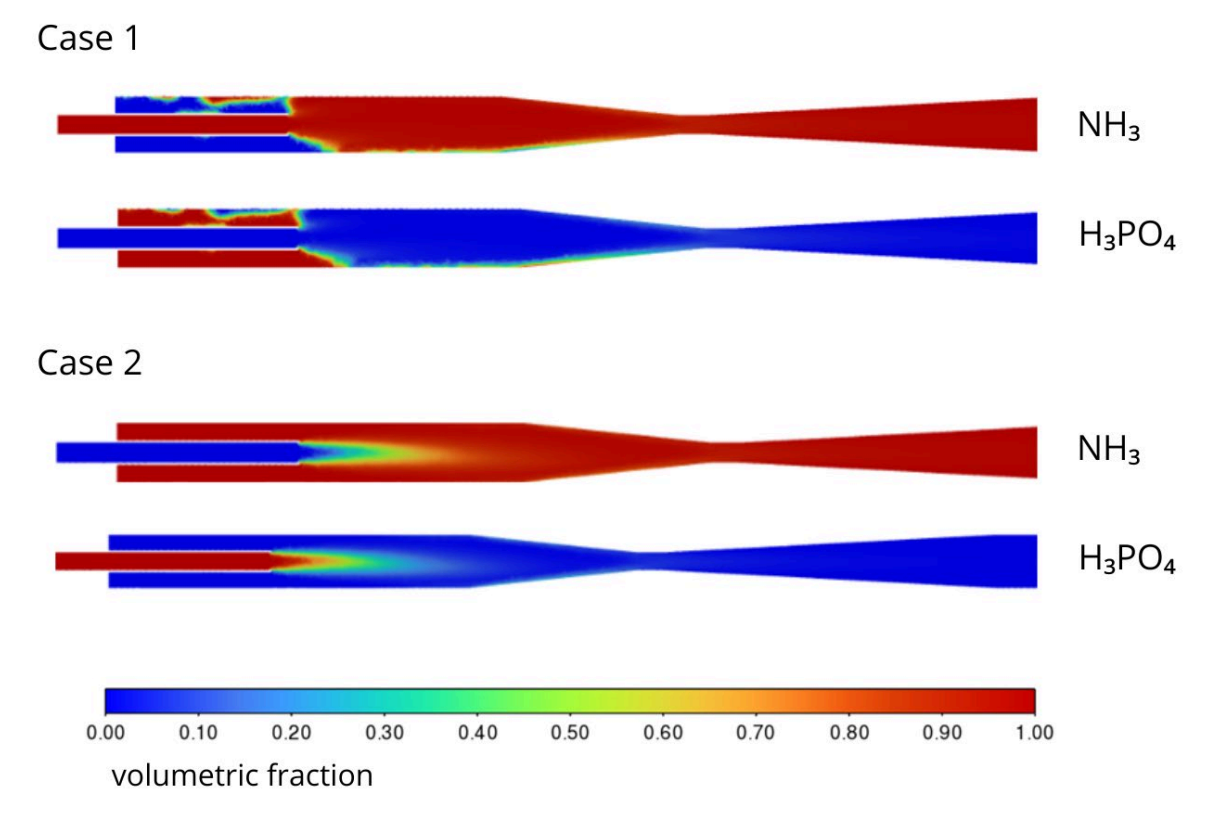


Figure 6. The volumetric fraction of ammonia and H_3PO_4 in the initial section of the tubular reactor for t = 2.0 s.

At the very inlet, both NH₃ and H₃PO₄ show distinct regions. For NH₃, the inlet pipe is predominantly at a volumetric fraction close to 1.00, indicating pure ammonia. For H₃PO₄, the main reactor body (where H₃PO₄ is introduced) is predominantly at a volumetric fraction close to 1.00, indicating pure phosphoric acid. This is expected as they are introduced as separate, unmixed streams. Immediately downstream of the inlet, where the two phases are meant to interact, there's a region where the volumetric fractions transition. For NH₃, this means a shift from volumetric fractions near 1.00 down to values between 0.20 and 0.50, indicating mixing of both phases. Similarly, for H₃PO₄, the presence of ammonia causes a shift from volumetric fractions near 1.00 towards values between 0.20 and 0.50 where ammonia is introduced. The volume fraction distributions of each phase in the inlet section differ due to the different locations of the ammonia and H₃PO₄ inlets streams for Case 1 and 2. The inlet velocity of ammonia is much higher than the orthophosphoric acid velocity. Additionally, the acid has a much higher density than ammonia, which is why it accumulates in the inlet part in Case 1. Then the acid is entrained in the lower part of the reactor and moves down towards the nozzle. Such a way of distributing the dispersed phase (H₃PO₄) does not favor the efficiency of the MAP formation reaction. Then the factors react only in the lower part of the reactor. The entire center of the reactor tube to the nozzle is filled only with ammonia, which can be seen in Figure 7 (Case 1). There, the reaction will not practically proceed.

It is different in Case 2 where orthophosphoric acid is fed to the pipe coaxial with the reactor (front inlet), and ammonia to the side inlet. Then the acid is fed centrally to the middle of the reactor and is carried away by the already flowing ammonia. Figures 6 and 7 (Case 2) show how the acid and ammonia mix in the middle of the reactor. This method of distributing and dispersing the acid in the ammonia stream is more effective due to the MAP formation reaction.



516

517

518

519

520

521

522

523

524

525

526

527

528

529

530

531

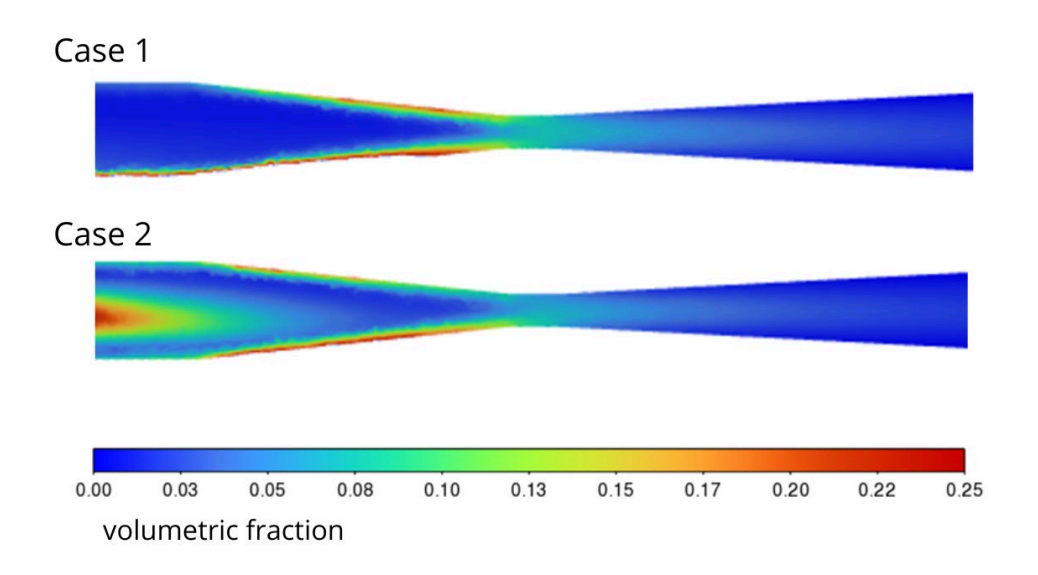
532

533

534

535

536



541	Figure 7. The volumetric fraction of H ₃ PO ₄ in the constriction section of the tubular reactor for
542	t = 2.0 s.
543	In Case 1, a single, central ammonia inlet creates a high-velocity jet. This design is effective
544	for deep penetration into the liquid phase but may result in slower mixing rates at the edges of
545	the jet due to the limited interfacial area. The instabilities observed at the interface suggest
546	shear-induced mixing, where the fast-moving ammonia jet interacts with the slower-moving
547	phosphoric acid. Conversely, in Case 2, the side inlet appear to promote a more immediate and
548	broader distribution of ammonia across the initial cross-section, with higher volumetric
549	fractions (e.g., $0.50-0.70$) spread over a wider area at the inlet. This configuration could
550	potentially lead to faster overall mixing and a larger interfacial area for reaction, as the ammonia
551	is less concentrated in a single core.
552	In both cases, as the mixture enters the converging nozzle, the ammonia phase (volumetric
553	fraction near 1.00) becomes highly concentrated in the core, and the H ₃ PO ₄ (volumetric fraction
554	near 0.00) appears to be pushed towards the walls, as is presented in Figure 7. This is a common
555	phenomenon in annular or core-annular flow regimes within nozzles, especially when a gas is
556	injected into a liquid. The gas (ammonia) tends to occupy the central, higher-velocity region,
557	while the liquid (H ₃ PO ₄) flows along the walls.
558	It can be observed that Case 2 might offer better initial mixing due to the broader distribution
559	of ammonia at the inlet. In Case 1, however, it may be necessary to redesign the reactor inlet
560	section to obtain better, more uniform mixing. Furthermore, the relatively sharp interface
561	observed between regions of high and low volumetric fraction in both cases, particularly within
562	the nozzle, indicates that complete molecular-level mixing may still be in its developmental
563	stages. The high velocities observed in Figures 3 and 4 are crucial here. Specifically, the high
564	velocity of the ammonia jet in Case 1, or the accelerated flow within the nozzle in both cases,
565	generates significant shear forces at the gas-liquid interface, which is important in driving the
566	dispersion of the gas phase in the liquid, thereby promoting efficient mixing.
567	Starting from the nozzle exit, the volumetric fraction of H ₃ PO ₄ is the same in the two cases
568	studied (Figure 7). Additionally, taking into account the velocity profiles of orthophosphoric
569	acid (Figure 4), it can be concluded that after passing through the nozzle, the mixture of acid
570	and ammonia has the same distribution and velocities. The situation is similar in both cases
571	studied.
572	Figure 8 illustrates the volumetric fraction distribution of H ₃ PO ₄ at the outlet of a tubular reactor
573	across five distinct simulation time points: 0.6 s , 1.0 s , , 2.0 s , and 3.0 s . In both cases show a
574	pronounced asymmetry in the H ₃ PO ₄ distribution. A significant portion of the cross-section

exhibits a volumetric fraction near 0.0, indicating a very low concentration or absence of H₃PO₄. Conversely, a crescent-shaped region on one side (right side in the figure) is predominantly at a volumetric fraction near 1.0, indicating a high concentration of H₃PO₄. This phenomenon can be explained by the assumed high velocity of ammonia, which entrains some of the dispersed phase droplets and, after passing through the constriction, impacts the rear wall of the reactor and then gravitationally falls towards the outlet. The much higher density acid flows down the rear wall of the reactor, which is visible in the cross-section of the reactor outlet in Figure 8. The low volumetric fraction on the opposite side implies that the ammonia is occupying that space. For each corresponding time step, the H₃PO₄ volumetric fraction distributions for Case 1 and Case 2 are almost similar. The degree of segregation, the shape of the high-concentration region, and the overall pattern are almost identical. As time progresses from 0.6 s to 1.0 s, 2.0 s, and 3.0 s, the general pattern of segregation persists.



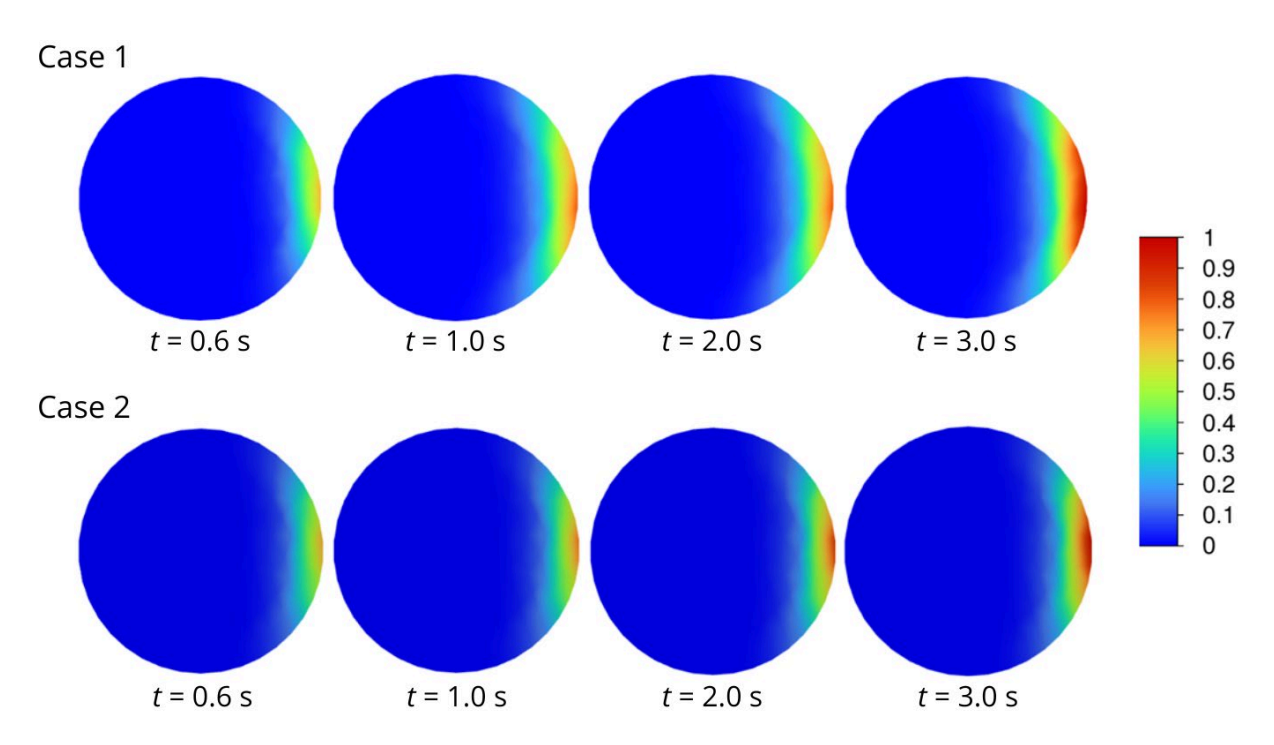


Figure 8. The volumetric fraction distribution of H₃PO₄ at the outlet of the tubular reactor across different simulation time steps.

Figure 9 was created to quantitatively evaluate the obtained simulation results. This figure presents the distribution of the liquid orthophosphoric acid within the reactor outlet along its diameter over time for both Case 1 and Case 2. Fig. 9 also shows sample contours of the volumetric fraction distribution of H_3PO_4 with the diameter marked in white for t = 3 s. The values presented in Fig. 9 refer to this diameter.

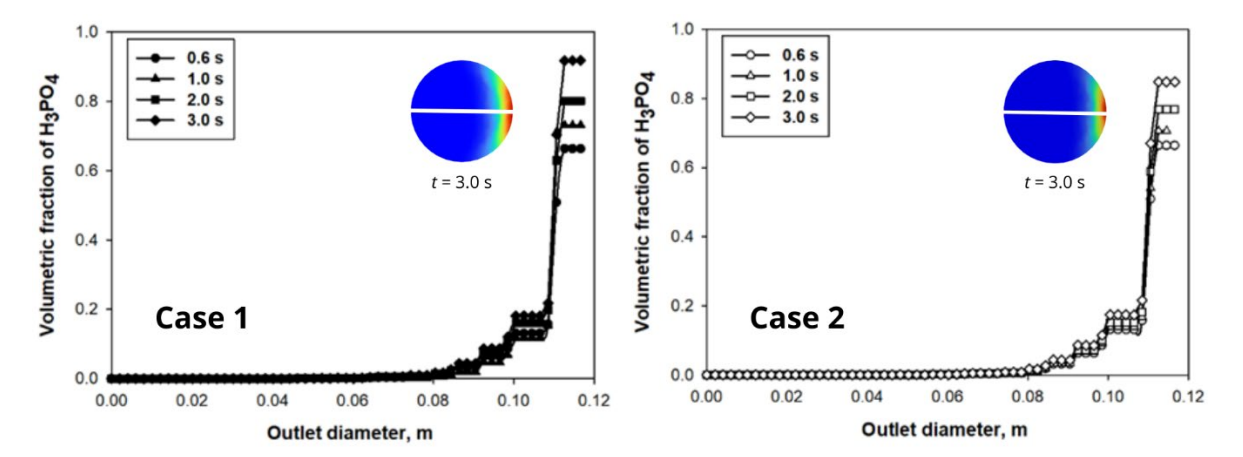


Figure 9. A comparison of the volumetric fraction of orthophosphoric acid as a function of the outlet diameter for Case 1 and Case 2.

The volume fraction of H₃PO₄ is negligible up to an outlet diameter of 0.08 m (Fig. 9) which corresponds to the blue area on the contours shown in Fig. 8 and increases rapidly towards the back wall, reaching a maximum value at an outlet diameter of approximately 0.12 m.

During the initial transient period (from t = 0.6 s to 1.0 s), the volumetric fraction profiles are still developing. The increases are consistent for both Case 1 and Case 2. The volumetric fraction increases by approximately 13% and 9% from 0.6 s to 1.0 s, for Case 1 and Case 2, respectively. The value of the volumetric fraction at the 3.0 s time step is approximately 0.9 (0.92 for Case 1 and 0.85 for Case 2).

In the real process, when the MAP formation reaction takes place, the MAP crystals formed should fall down in this part of the reactor. It seems that then the volumetric fraction distribution of MAP at the reactor outlet should be different. MAP crystals should occupy a larger part of the outlet pipe. It is likely that including chemical species transport equations in the calculations, taking into account chemical reaction kinetics, would allow for obtaining a more accurate picture of the volume distribution of both phases and observing the appearance of the reaction product at the reactor outlet.

5. CONCLUSIONS

In conclusion, the simplified computational approach presented here offers a practical tool for understanding and optimizing hydrodynamic behavior in tubular reactors for MAP production. The simulation results provide valuable information on reactant distribution and mixing,

directly relevant to reactor performance. The ability to visualize and quantify these phenomena allows for informed design decisions regarding inlet configurations, reactor dimensions, and operating parameters. This knowledge can be used to mitigate issues such as poor mixing or channeling, leading to a more efficient and cost-effective MAP production process.

The following specific conclusions were drawn based on the simulation results:

- The analyses of velocity profiles and volumetric fraction distributions, as illustrated in Figures 3, 4, and 5, highlight the significant impact of key parameters on reactor performance. Volumetric flow rates, fluid physicochemical properties, reactor geometry, operating conditions, and initial phase distribution all play critical roles in determining flow regimes and mixing efficiency. Crucially, the study emphasized the practical implications of these findings. The ability to visualize and quantify the distribution of H₃PO₄ at different time steps, as shown in Figures 4 and 5, provides essential data for optimizing reactor design and operation.
 - A significant effect of the reactant dosing location into the reactor was observed and was more effective in Case 2 with respect to the MAP formation reaction. In Case 1 ammonia was supplied to the reactor from the front of the reactor, while orthophosphoric acid flowed through the side inlet. Due to the much higher velocity of ammonia relative to acid and the significantly higher density of acid than ammonia, accumulation of acid was observed in the inlet section. Then, the acid was entrained in the lower part of the reactor and moved down towards the nozzle. Such a way of distributing the dispersed phase (H₃PO₄) does not favor the efficiency of the MAP formation reaction. Then the factors will react only in the lower part of the reactor. The entire center of the reactor tube up to the nozzle was filled only with ammonia (Figure 7), so practically no reaction will occur there. In Case 2, conversely, phosphoric acid flowed through the main inlet and ammonia through the side inlet. The acid was fed centrally into the reactor and discharged with the already flowing ammonia. There was a much better mixing of the reactants in the inlet section of the nozzle (Figs. 6 and 7). This method of distributing and dispersing the acid in the ammonia stream is more effective with respect to the MAP formation reaction.
- High ammonia and acid velocities were obtained at the constriction (nozzle) in the reactor tube. The nozzle design caused a uniform discharge of the reactants to the further part of the reactor, where there was good mixing of the components, comparable to Cases 1 and 2. Good mixing of the components was obtained, and thus good conditions for carrying out the MAP formation reaction. Further numerical studies should be

- carried out, supplemented by modeling of the reaction in the reactor. Then it will be possible to observe whether the length of the reactor from the constriction to the 90-degree elbow is sufficient for the complete MAP reaction.
- A persistent phase segregation of H₃PO₄ is observed at the reactor outlet concentrating H₃PO₄ on one side (volumetric fraction near 1.0) and leaving the other side with very low H₃PO₄ (near 0.0). This segregation is largely unaffected by the initial ammonia inlet design and does not diminish over time. In the real process, when the MAP formation reaction takes place, the MAP crystals formed should fall down in this part of the reactor and they should occupy a larger part of the outlet pipe. It is likely that including chemical species transport equations in the calculations, taking into account chemical reaction kinetics, would allow for obtaining a more accurate picture of the volume distribution of both phases and observing the appearance of the reaction product at the reactor outlet.
- The presented modeling results can be used to optimize the design of tubular reactors
 for efficient mixing of gas and liquid phases. By visualizing the distribution of reactants,
 the inlet configurations can be adjusted, reactor dimensions, and flow rates to achieve
 desired mixing patterns.

These simulations are a powerful tool to optimize reactor design by adjusting inlet configurations and internal structures to enhance turbulence and ensure consistent reactant distribution. Understanding liquid phase residence time is vital for process control and product quality. These insights are indispensable for successful reactor scale-up. The study underscores the importance of fluid properties and operating conditions on flow patterns and reaction kinetics. Future simulations should integrate chemical species transport and reaction kinetics for more accurate predictions and a comprehensive understanding of the reaction process. Ultimately, the data presented in this study provides valuable insights into the hydrodynamic behavior of tubular reactors, empowering engineers to make informed decisions for optimizing reactor design and operation. By understanding and controlling the factors influencing fluid dynamics, we can improve mixing efficiency, enhance product quality, and ensure the successful production of MAP fertilizer and other related chemical processes.

685 SYMBOLS

 C_D - drag coefficient

 d_b - droplet diameter of dispersed phase, μm

 F_k – the interphase force, kg/(m²·s²)

P – pressure, N/m² 689 690 $P_{k,m}$ - rate of production of turbulent kinetic energy 691 k – kinetic energy of turbulence, m²/s² 692 K – interphase momentum exchange coefficient, kg/(m³·s) Rez – relative Reynolds number 693 694 t – time, s 695 u – velocity, m/s 696 697 Greek symbols 698 α – volume fraction 699 Δt – time step, s ε - energy dissipation rate, m²/s³ 700 701 μ , μ_{eff} , μ_t – molecular, effective and turbulent dynamic viscosity, kg/(m·s²) 702 $\mu_{t,m}$ - the turbulent viscosity, kg/(m·s²) 703 ρ – density, kg/m³ 704 705 **Subscripts** 706 *k* –phase 707 l – liquid 708 g - gas709 m - mixture710 711 **REFERENCES** 712 Andrade A.D., Ferraz G.A.S., de Barros M.M., Faria R.D., da Silva F.M., Sarri D., Vieri M., 713 2020. Characterization of the transverse distribution of fertilizer in coffee plantations. 714 Agronomy, 10, 601. DOI: 10.3390/agronomy10040601. 715 Belis D., Chinal P., Priat J.F., 1986. Production of ammonium phosphates containing 716 ammonium sulphate. EP0272183A1. Bortoletto-Santos R., Plotegher F., Roncato V., Majaron R.F., Majaron V.F., Polito W.L., 717 718 Ribeiro C., 2018. Strategy for multinutrient application in integrated granules using zein

as a coating layer. J. Agric. Food Chem., 2018, 66, 9582-9587. DOI:

719

720

10.1021/acs.jafc.8b01319.

- 721 Chemical Book, 2025. Ammonium dihydrogen phosphate. Available at:
- https://www.chemicalbook.com/chemicalproductproperty en cb6131092.htm access
- 723 date 27/07/2020
- 724 Dhanasekharan K.M., Sanyal J., Jain A., Haidari A., 2005. A generalized approach to model
- oxygen transfer in bioreactors using population balances and computational fluid
- 726 dynamics. *Chem. Eng. Sci.*, 60, 213–218. DOI: 10.1016/j.ces.2004.07.118.
- 727 Edelbauer W., 2017. Numerical simulation of cavitating injector flow and liquid spray break-
- up by combination of Eulerian-Eulerian and Volume-of-Fluid methods. Comput. Fluids,
- 729 144, 19–33, 2017. DOI: 10.1016/j.compfluid.2016.11.019.
- 730 Eltarabily M.G., Burke J.M., Bali K.M., 2019. Effect of deficit irrigation on nitrogen uptake of
- sunflower in the low desert region of california. Water, 11, 2340. DOI:
- 732 10.3390/w11112340.
- 733 Gargouri M., Chtara C., Charock P., Nzihou A., Elfeki H., 2010. Synthesis and
- physicochemical characterization of pure monoammonium phosphate (MAP) from
- industrial fertilizer. J. Chem. Chem. Eng., 49(6), 49–57.
- Gargouri M., Chtara C., Sharrock P., Nzihou A., El Feki H., 2012. Experimental study of the
- purification of an industrial fertilizer (mono-ammonium phosphate) to larger scale using
- 738 an experimental design. *Int. J. Mater. Eng.*, 2, 32–37. DOI: <u>10.5923/j.ijme.20120204.01</u>.
- Havelange, S., Van Lierde, N., Germeau, A., Martins, E., Theys, T., Sonveaux, M., Toussaint,
- C., Schrödter, K., Bettermann, G., Staffel, T., Wahl, F., Klein, T. and Hofmann, T.
- 741 (2023). Phosphoric Acid and Phosphates. In: Ullmann's Encyclopedia of Industrial
- 742 *Chemistry*. DOI: 10.1002/14356007.a19 465.pub4.
- 743 Hebei Toprun Chemical Industry, 2004. Preparation method of nitrogen phosphorus or
- 744 nitrogen phosphorus potassium composite fertilizer. CN1303041C.
- Hudson J.W., Pendergrast R.A., 1975. Process for the manufacture of monoammonium
- 746 *phosphate*. US4009245A.
- 747 Icardi M., Ronco G., Marchisio D.L., Labois M., 2014. Efficient simulation of gas-liquid pipe
- flows using a generalized population balance equation coupled with the algebraic slip
- 749 model. *Appl. Math. Modell.*, 38, 4277–4290. DOI: 10.1016/j.apm.2014.04.052
- Jakobsen H.A., 2008. Chemical reactor modelling. Multiphase reactive flows. Springer-Ferlag,
- 751 Berlin, Heidelberg.
- Kabiri S., Andjelkovic I.B., da Silva R.C., Degryse F., Baird R., E. Tavakkoli, D. Losic, M. J.
- McLaughlin, 2020. Engineered phosphate fertilizers with dual-release properties. *Ind. Eng.*
- 754 Chem. Res., 59, 5512–5524. DOI: 10.1021/acs.iecr.0c00403.

- 755 Kerdouss F., Bannari A., Proulx P., 2006. CFD modeling of gas dispersion and bubble size in
- a double turbine stirred tank. Chem. Eng. Sci., 61, 3313-3322. DOI:
- 757 10.1016/j.ces.2005.11.061
- 758 Launder B.E., Spalding D.B., 1972. Lectures in mathematical models of turbulence. Academic
- 759 Press, London, UK.
- Lino A.C.M., Buzetti S., Teixeira Filho M.C.M., Galindo F.S., Maestrelo P.R., de Carvalho
- Rodrigues M.A., 2018. Effect of phosphorus applied as monoammonium phosphate-coated
- polymers in corn culture under no-tillage system. Semina Cienc. Agrar., 39, 99–112. DOI:
- 763 <u>10.5433/1679-0359.2018v39n1p99</u>.
- 764 Liu Z., Zhao Q., Wie L., Wu D., Ma L., 2011. Effect of struvite seed crystal on MAP
- 765 crystallization. J. Chem. Technol. Biotechnol., 86, 1394–1398. DOI: 10.1002/jctb.2716.
- Lombi E., McLaughlin M.J., Johnston C., Armstrong R.D., Holloway R.E., 2004. Mobility and
- lability of phosphorus from granular and fluid monoammonium phosphate differs in a
- 768 calcareous soil. *Soil Sci. Soc. Am. J.*, 68, 682–689. DOI: 10.2136/sssaj2004.6820.
- 769 Mpountas I., Papadakis E., Koutsoukos P., 2017. Phosphorus recovery from simulated
- municipal wastewater (SMW) through the crystallization of magnesium ammonium
- phosphate hexahydrate (MAP). J. Chem. Technol. Biotechnol., 92, 2075–2082, 2017. DOI:
- 772 <u>10.1002/jctb.5202</u>.
- Nyers J.M., Rawlings G. D., Mullen E. A., Moscowitz C. M, Reznik R. B., 1979. Source
- assessment: phosphate fertilizer industry, EPA-600/2-79-019c. U.S. Environmental
- Protection Agency, Industrial Environmental Research Laboratory, National Technical
- 776 Information Service. Available at:
- https://nepis.epa.gov/Exe/ZyPDF.cgi?Dockey=91017T0A.PDF.
- Patankar S.V., 1980. Numerical heat transfer and fluid flow. CRC Press. DOI:
- 779 10.1201/9781482234213.
- 780 Picardi R., Zhao L., Battaglia F., 2016. On the ideal grid resolution for two-dimensional
- 781 eulerian modeling of gas-liquid flows. J. Fluids Eng., 138, 114503. DOI:
- 782 <u>10.1115/1.4033561</u>.
- Prosperetti A., Jones A., 1987. The linear stability of general two-phase flow models–II. *Int. J.*
- 784 *Multiphase Flow*, 13, 161–171. DOI: <u>10.1016/0301-9322(87)90027-9</u>.
- Ramkrishna D., 2000. Population balances: Theory and applications to particulate systems in
- 786 engineering. Academic Press, San Diego, USA.

- 787 Rzehak R., Krepper E., Lifante C., 2012. Comparative study of wall-force models for the
- simulation of bubbly flows. Nucl. Eng. Des., 253, 41–49. DOI:
- 789 <u>10.1016/j.nucengdes.2012.07.009.</u>
- 790 Schiller L., Naumann Z., 1935. Über die grundlegenden Berechnungen bei der
- 791 Schwerkraftaufbereitung. Zeitschrift des Vereins Deutscher Ingenieure, 77, 318–320.
- 792 Shanghai Research Institute of Chemical Industry SRICI, 2006. Method for manufacturing
- 793 powdered granulated potassium ammonium sulfate compound fertilizer. CN101200392B.
- 794 Tennessee Valley Authority, 1987. Diammonium phosphate produced with a high-pressure
- 795 *pipe reactor*. US4758261A.
- 796 Timilsena Y.P., Adhikari R., Casey P., Muster T., Gill H., Adhikari B., 2015. Enhanced
- 797 efficiency fertilisers: a review of formulation and nutrient release patterns. J. Sci. Food
- 798 *Agric.*, 95, 1131–1142. DOI: 10.1002/jsfa.6812.
- 799 UN Industrial Development Organization, Int'l Fertilizer Development Center, 1998. Fertilizer
- 800 *Manual*. 3rd edition, Springer Netherlands.
- Xue B.C., Hao Q., Liu T., Liu E.B., 2013. Effect of process parameters and agglomeration
- mechanisms on NPK compound fertiliser. *Powder Technol.*, 247, 8–13. DOI:
- 803 <u>10.1016/j.powtec.2013.06.027.</u>
- Yara International ASA, 2005. Pipe reactor and plant for manufacturing of especially urea
- ammonium sulphate. US20080145283A1.